Theoretical study of the magnetic order in α-CoV_2O_6

A. Saúl* and D. Vodenicarevic
CINaM, UMR 7325 CNRS, Aix-Marseille University, Campus de Luminy, 13288 Marseille cedex 9, France

G. Radtke†
IM2NP, UMR 7334 CNRS, Aix-Marseille University, Faculté des Sciences de Saint-Jérôme, F-13397 Marseille, France
(Received 6 July 2012; revised manuscript received 23 December 2012; published 7 January 2013)

The electronic structure and magnetic properties of α-CoV_2O_6 are investigated using density functional theory calculations including spin-orbit coupling and orbital polarization effects. These calculations reveal a strong magnetocrystalline anisotropy with a magnetization easy axis close to the *c* axis. The evaluation of magnetic couplings on the basis of broken-symmetry formalism suggests the occurrence of an antiferromagnetic ground-state order where ferromagnetic chains running along *b* are coupled antiferromagnetically to their nearest neighbors along *a* and *c*. Monte Carlo simulations are finally employed to explore the origins of the 1/3 plateau observed in the magnetization curves of this compound and to propose a structure for the corresponding state.

DOI: 10.1103/PhysRevB.87.024403 PACS number(s): 75.30.Et, 71.20.Ps, 75.10.Dg

I. INTRODUCTION

Co-based spin-chain compounds often display fascinating magnetic properties and provide a wide range of real material systems susceptible to test models developed in condensed-matter physics. For example, $CoNb_2O_6$, a compound built from weakly coupled ferromagnetic zigzag Co chains, has recently allowed the experimental observation of a quantum phase transition of the one-dimensional Ising chain in a transverse field.[1,2] Geometry, magnetic couplings, or single-ion anisotropy are the fundamental ingredients that eventually determine the specific magnetic behavior of these compounds. Their theoretical study is therefore crucial when interpreting the observed magnetic properties but also for the design of new systems.

In this paper, we focus our attention on CoV_2O_6, a compound that has been the subject of a series of recent experimental investigations.[3–7] This compound crystallizes under two distinct polytypes,[5,8,9] triclinic γ-CoV_2O_6 and monoclinic α-CoV_2O_6. We will restrict our study to the second phase only, which crystallizes in the branneritelike monoclinic structure with space group $C2/m$[8] depicted in Fig. 1(a). In this structure, the formally divalent cobalt ions ($3d^7$) are located in distorted octahedra sharing edges so as to form linear chains running along the *b* crystallographic axis. These chains are linked together through VO_5 square pyramids involving pentavalent, and therefore nonmagnetic ($3d^0$), vanadium ions. Experimental investigations of the magnetic properties of α-CoV_2O_6 established the basic features of this compound:[4,5] (i) a transition to an antiferromagnetic (AF) order occurring at 15 K, (ii) a large magnetic anisotropy with a magnetic easy axis oriented along the crystallographic *c* axis, i.e., perpendicular to the chain direction, (iii) a metamagnetic behavior characterized by two steps in the magnetization curve delimiting a plateau at 1/3 of the saturation magnetization in the absence of an obvious triangular or kagome-type lattice, and (iv) a saturation magnetization of (4.5–4.6)μ_B/Co^{2+} ion indicative of a large orbital contribution.

Most of the classical works[10–12] devoted to the study of the magnetic properties of octahedrally coordinated Co^{2+} tackled this problem on the basis of a crystal-field analysis. Under the combined effect of tetragonal (or trigonal) distortion of the cubic crystal field and spin-orbit (SO) coupling, the ground state of the ion appears to be a Kramers doublet located well below the higher energy levels. This result led to interpretations of the magnetic properties of compounds containing this ion as systems of strongly anisotropic effective spin 1/2. Although this single-ion model is very powerful to justify the Ising nature typical of Co^{2+}-based compounds, it is obviously unable to shed light on collective properties such as long-range magnetic ordering. In this paper, we propose a different approach based on density functional theory (DFT) calculations beyond standard generalized gradient approximation (GGA) and Monte Carlo simulations to investigate the electronic structure and magnetic properties of α-CoV_2O_6. In particular, we show that the effective exchange interactions obtained from the DFT calculations correctly predict the AF ground state and allow an understanding of the specific magnetic order corresponding to the 1/3 magnetization plateau.

II. CALCULATION METHOD

Electronic structure and total energy calculations were performed using the WIEN2K code.[13] This program is an implementation of the full-potential linearized augmented plane-wave method based on density functional theory. The calculations presented hereafter were performed using the generalized gradient approximation of Perdew, Burke, and Ernzerhof[14] for exchange and correlation and a cutoff parameter $RK_{max} = 7$. The radii of the muffin-tin spheres were set to 1.97 a.u. for Co, 1.65 a.u. for V, and 1.47 a.u. for O in all of these calculations. Spin-orbit coupling, when included, was treated using scalar-relativistic wave functions in a second-variational procedure[15] and orbital polarization (OP) effects were treated using the *ad hoc* correction proposed by Brooks.[16]

III. RESULTS

A. Electronic structure

The spin-polarized projected density of states (PDOS) for Co, V, and O atoms in α-CoV_2O_6 are shown in Fig. 2(a).

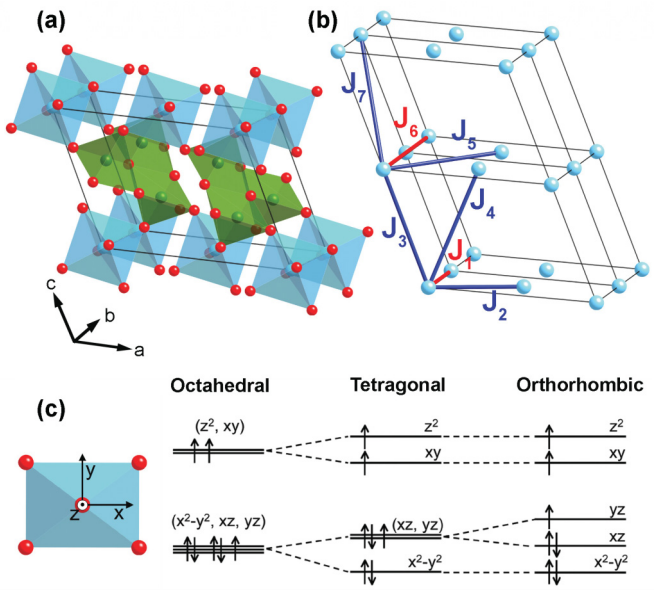

FIG. 1. (Color online) (a) Atomic structure of α-CoV_2O_6: Red balls denote oxygen ions, CoO_6 octahedra are shown in blue, and VO_5 square pyramids in green. (b) Magnetic couplings in α-CoV_2O_6. Intrachain couplings (J_1 and J_6) are shown in red and interchain couplings (J_2, J_3, J_4, J_5, and J_7) are shown in blue. (c) Splitting of the Co 3d levels illustrating successively the effects of the tetragonal and orthorhombic distortions of the Co coordination octahedron.

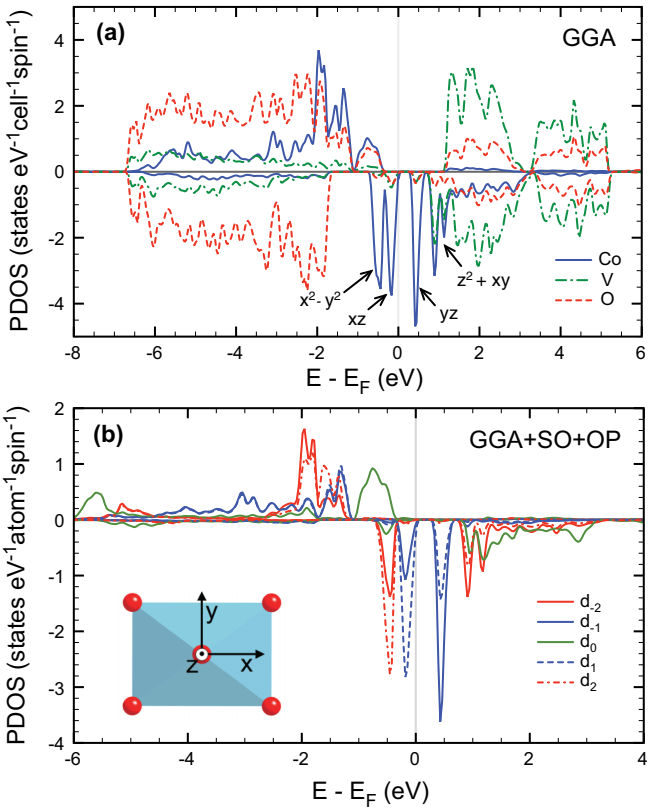

FIG. 2. (Color online) (a) Co, V, and O projected densities of states calculated in the GGA with the experimental crystal structure and a ferromagnetic arrangement of the Co magnetic moments in α-CoV_2O_6; (b) Co 3d projected density of states calculated with the GGA + SO + OP decomposed on complex d_m orbitals. For symmetry reasons, a nonconventional orientation of the local system of coordinates has been chosen.

This calculation has been performed for a ferromagnetic arrangement of the Co magnetic moments and for the experimental crystal structure. This compound appears as a semiconductor with a band gap of 0.25 eV occurring between minority-spin crystal-field-split Co 3d states. The specific splitting of the one-electron Co 3d orbitals visible in the PDOS can be understood with the help of Fig. 1(c). A first dominant tetragonal distortion associated with a contraction ($\approx$10%) of the bond length between the apical oxygen and the Co ions is first responsible for the $d_{x^2-y^2}$-(d_{xz},d_{yz}) and d_{z^2}-d_{xy} splitting. Then, an orthorhombic distortion in the equatorial plane further lifts the d_{xz}-d_{yz} degeneracy.

It should be noted here that due to the orthorhombic distortion, a nonconventional orientation of the local system of coordinates has been chosen, as indicated in Fig. 1(c). With this choice, the z axis is slightly off the crystallographic c axis by an angle of 9° in the ac plane. The x direction is parallel to the chain direction, i.e., the crystallographic b axis. It can be clearly seen here that Co^{2+} ions adopt a high-spin (HS) $S = 3/2$ electronic configuration, giving rise to a magnetic moment of $3\mu_B$/Co ion or $2.52\mu_B$ inside the Co muffin-tin sphere. In our local system of coordinates, the two occupied minority-spin 3d orbitals are therefore $d_{x^2-y^2}$ and d_{xz}. To confirm that this particular orbital occupation scheme indeed corresponds to the lowest-energy electronic state of the divalent Co ion in this compound, additional calculations have been carried out by stabilizing either a second HS configuration where the minority-spin d_{yz} is occupied instead of d_{xz} or a low-spin (LS) $S = 1/2$ configuration. These configurations are found respectively 140 and 460 meV/f.u. higher in energy, confirming the ground-state nature of the electronic structure shown in Fig. 2(a). Calculations performed for an AF arrangement[17] of the Co ions in both the HS and LS states confirm the stabilization of the HS state by the same energy difference. We thus conclude that the HS state is the low-energy configuration for the Co ion independently of the specific magnetic order. As a gap in the electronic DOS is already found in the GGA, giving an acceptable description of this magnetic insulator, the calculations shown hereafter have been carried out using the same exchange-correlation functional.

B. Magnetic anisotropy

To examine the magnetocrystalline anisotropy of HS Co^{2+} in this compound, and in particular to determine the magnetization easy axis, GGA + SO calculations were carried out. The DFT total energy dependence upon the Co magnetization orientation has been systematically calculated in the bc and the ac planes in the framework of collinear magnetism. These calculations give an anisotropy of 1.8 meV/Co ion and a minimum when the magnetization is oriented along the local z axis, i.e., close to the crystallographic c axis in agreement with the experiments.[4,7] The corresponding orbital magnetic moment is $0.2\mu_B$ and parallel to the spin-only magnetic moment as the 3d electronic shell is more than half filled. These results can be readily understood by considering the

Co^{2+} crystal-field levels shown in Fig. 1(c) and treating the SO coupling as a perturbation. As the exchange splitting is large enough to separate majority from minority spins relatively well in energy, we can consider only the spin-conserving part of the SO Hamiltonian $\hat{H}_{\rm SO} = \xi \hat{\mathbf{L}} \cdot \hat{\mathbf{S}}$ in our analysis. For an orientation of the magnetization along the $\mathbf{n}(\theta,\phi)$ direction (θ and ϕ are respectively the polar and azimuthal angles in our local coordinate system), we therefore write

$$\hat{H}_{\rm SO} \approx \xi \hat{S}_n \left(\hat{L}_z \cos\theta + \frac{1}{2} \sin\theta [\hat{L}_+ e^{-i\phi} + \hat{L}_- e^{i\phi}] \right). \quad (1)$$

The leading terms in the second-order nondegenerate perturbation expansion imply matrix elements $\langle d^{\downarrow}_{xz} | \hat{H}_{\rm SO} | d^{\downarrow}_{yz} \rangle \propto i\frac{\xi}{2} \cos\theta$ and $\langle d^{\downarrow}_{x^2-y^2} | \hat{H}_{\rm SO} | d^{\downarrow}_{xy} \rangle \propto i\xi \cos\theta$, maximizing the SO stabilization for $\theta = 0^\circ$ and thus fixing the magnetization along the local z axis. If this approach confirms the orientation of the experimental magnetization easy axis, it also largely underestimates the orbital magnetic moment and might be interpreted as a failure of the GGA to respect Hund's second rule for Co in this compound. The addition of a Hubbard U to the GGA functional does not correct the problem. Indeed this approach reduces the magnetic anisotropy and consequently the orbital contribution to the magnetic moment. The reason is that it increases the gap and consequently the energy difference between the states responsible for the leading terms in the perturbative expansion of the spin-orbit interaction. In order to remedy this deficiency, we used the orbital polarization correction proposed by Brooks[16] as implemented in WIEN2K. The results confirm the orientation of the magnetic easy axis but enhance the magnetic anisotropy by two orders of magnitude, giving an upper estimate of 130 meV/Co ion and leading to an orbital contribution to the total magnetic moment of $0.93\mu_B$. The large imbalance in the weights of the $d_{\pm1}$ and $d_{\pm2}$ complex orbitals associated with the appearance of this orbital moment can be readily seen in the decomposition of the Co $3d$ LDOS presented in Fig. 2(b). Despite a seemingly large overestimation of the magnetic anisotropy, orbital polarization corrections nevertheless prove necessary to get an overall better description of the magnetic behavior of this compound.

C. Magnetic order

To get further insight into the macroscopic magnetic properties of α-CoV_2O_6, we evaluated magnetic couplings in this compound on the basis of broken-symmetry formalism, i.e., based on the computation of total energies for supercells characterized by different collinear arrangements of the Co^{2+} magnetic moments. Taking into account the Ising-type behavior dominating the phenomenology of α-CoV_2O_6, we modeled the magnetic excitations in this compound with the following Hamiltonian:

$$\hat{H} = \hat{H}_0 - D \sum_i \hat{S}^2_{iz} + \sum_{i>j} J^{\parallel}_{ij} \hat{S}_{iz} \hat{S}_{jz} + J^{\perp}_{ij} (\hat{S}_{ix} \hat{S}_{jx} + \hat{S}_{iy} \hat{S}_{jy}), \quad (2)$$

where $\hat{H}_0$ is the spin-independent part of the Hamiltonian, $\hat{\mathbf{S}}_i$ and $\hat{\mathbf{S}}_j$ represent the spin-3/2 operators associated with sites i and j, respectively, D is the spin anisotropy parameter, and $J^{\parallel,\perp}_{ij}$ are the anisotropic magnetic couplings to calculate. In this work, exchange couplings up to the seventh nearest neighbors, i.e., within a maximum Co-Co distance of 8 Å, have been calculated and are shown in Fig. 1(b). In order to extract such a large number of couplings, two distinct supercells A ($1 \times 2 \times 2$) and B ($1 \times 4 \times 1$) have been employed.

The expectation value of (2) on the configuration k of the supercell $S = A, B$ is then

$$\epsilon^S_k(\mathbf{n}) = \epsilon^S_0(\mathbf{n}) - \frac{9}{4} N D \delta_{\parallel,\mathbf{n}} + \frac{9}{4} \sum_{i>j} J^{\mathbf{n}}_{ij} \sigma_i \sigma_j, \quad (3)$$

where $\epsilon^S_0(\mathbf{n})$ is the spin-independent part of the total energy, $\mathbf{n}$ is the magnetization direction in the local coordinate system, taken either parallel ($\parallel$) or perpendicular ($\perp$) to the magnetic easy axis, N is the number of magnetic ions in the supercell, and $\sigma_i = \pm 1$.

The two 72-atom supercells contain $N = 8$ magnetic ions leading, in each case, to a total of $2^8 = 256$ possible configurations. Taking spin reversal and crystalline symmetries into account, the number of independent configurations reduces to 22 for the $1 \times 2 \times 2$ supercell and 18 for the $1 \times 4 \times 1$ supercell. The total energies for the magnetic configurations in the A or B supercells can be written respectively as

$$\epsilon^A_k(\mathbf{n}) = \epsilon^A_0(\mathbf{n}) - \frac{9}{4} N D \delta_{\parallel,\mathbf{n}} + \frac{9}{4} \big[8 J^{\mathbf{n}}_6 + c^A_1 J^{\mathbf{n}}_1 + c^A_2 \big(J^{\mathbf{n}}_2 + J^{\mathbf{n}}_5 \big) + c^A_3 J^{\mathbf{n}}_3 + c^A_4 J^{\mathbf{n}}_4 + c^A_7 J^{\mathbf{n}}_7 \big] \quad (4)$$

and

$$\epsilon^B_k(\mathbf{n}) = \epsilon^B_0(\mathbf{n}) - \frac{9}{4} N D \delta_{\parallel,\mathbf{n}} + \frac{9}{4} \big[8 J^{\mathbf{n}}_3 + c^B_1 J^{\mathbf{n}}_1 + c^B_2 \big(J^{\mathbf{n}}_2 + J^{\mathbf{n}}_4 \big) + c^B_5 J^{\mathbf{n}}_5 + c^B_6 J^{\mathbf{n}}_6 + c^B_7 J^{\mathbf{n}}_7 \big]. \quad (5)$$

Supercell A does not allow calculation of J_6 and separation of J_2 and J_5, and in a similar way, it is not possible to calculate J_3 and to separate J_2 and J_4 using supercell B. Both supercells were therefore needed to unambiguously determine all the seven couplings by minimizing the following error function:[18]

$$E(\mathbf{n}) = \sum_{S=A,B} \sum_k g^{\rm S}_k \left[\epsilon^{\rm S}_k(\mathbf{n}) - \epsilon^{\rm S}_0(\mathbf{n}) + \frac{9}{4} N D \delta_{\parallel,\mathbf{n}} - \frac{9}{4} \sum_l c^{\rm S}_l(k) J^{\mathbf{n}}_l \right]^2, \quad (6)$$

where $g^{\rm S}_k$ is the degeneracy of the configuration k, i.e., the number of equivalent configurations. The spin-independent contributions to the total energy can be calculated as the weighted average of the calculated energies:

$$\epsilon^S_0(\mathbf{n}) = \frac{9}{4} N D \delta_{\parallel,\mathbf{n}} + \frac{1}{2^N} \sum_k g^S_k \epsilon^S_k(\mathbf{n}), \qquad S = A, B. \quad (7)$$

The resulting fits of the total energies in a GGA + SO + OP calculation with the magnetization parallel and perpendicular to the easy axis are shown in Fig. 3. A summary of the corresponding magnetic couplings is presented in Fig. 4.

Three magnetic interactions dominate the low-temperature behavior of this compound: a ferromagnetic intrachain interaction $J^{\parallel}_1 = -29.8$ K and two AF interchain interactions $J^{\parallel}_2 = 4.9$ K along a and $J^{\parallel}_3 = 10.6$ K along c. The corresponding

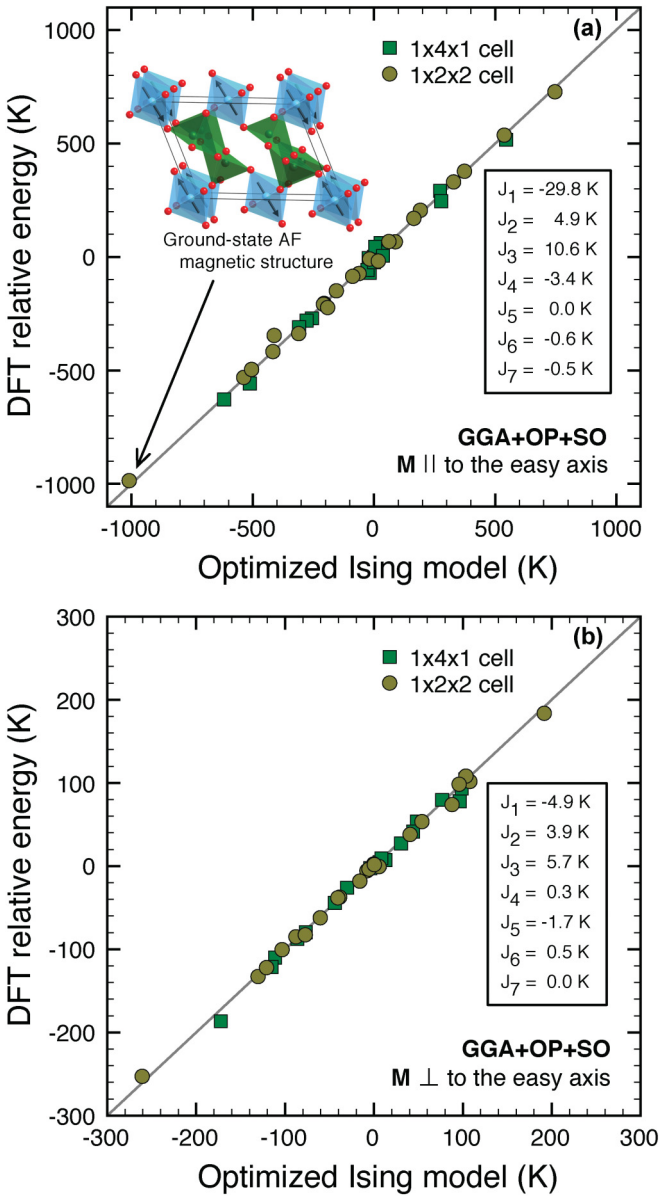

FIG. 3. (Color online) Graphical representation of the results obtained using the least-squares fit procedure: for each configuration, the DFT relative energy is represented as a function of the optimized Ising energy. The best-fit values are shown in the inset. According to the convention used in Eq. (2), positive couplings correspond to AF interactions. (a) Magnetization along the easy axis. (b) Magnetization perpendicular to the easy axis.

magnetic couplings for a direction of the magnetization perpendicular to the easy axis are systematically weaker.

These calculations lead to two important conclusions. First, they suggest a collinear AF structure characterized by a (0,0,1/2) propagation vector as the magnetic ground state for α-CoV_2O_6. In this structure, ferromagnetic chains running along b are coupled antiferromagnetically to the nearest chains in a and c directions. This magnetic order [see the inset of Fig. 3(a)] is in agreement with the structure determined recently[17] by neutron diffraction for this compound. Second, within the specific geometry of this compound, frustration can occur only in the presence of long-range magnetic interactions

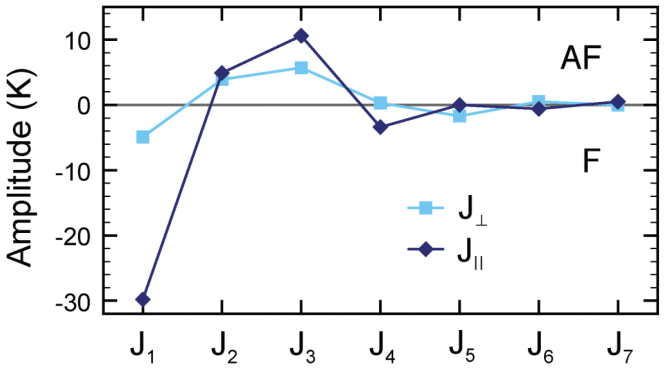

FIG. 4. (Color online) (a) Magnetic couplings computed in α-CoV_2O_6 up to the seventh-nearest neighbor for a direction of the magnetization along or perpendicular to the magnetic easy axis.

beyond third-nearest neighbors, i.e., beyond a Co-Co distance of 6.6 Å. As shown in Fig. 4, the computed values for these interactions are negligible with the exception of $J_4^{\parallel} = -3.4$ K. As already pointed out,[7,19] the interchain interactions J_2, J_3, and J_4 define a triangular network in a plane perpendicular to the ferromagnetic chains which could possibly be at the origin of the magnetization plateau observed for α-CoV_2O_6.[19] This is however based on the assumption that all these interactions are antiferromagnetic, in contradiction with our results for J_4. However, the weak amplitude of this interaction, close to the accuracy limit of our method, as well as the neglect of potentially large magnetoelastic coupling effects,[7,17] can reasonably justify the reassessment of J_4 to a weak antiferromagnetic value.

To test this hypothesis, we have used the magnetic couplings determined by the broken-symmetry procedure with the exception of $J_4^{\parallel}$ set to 2 K. The system was therefore modeled

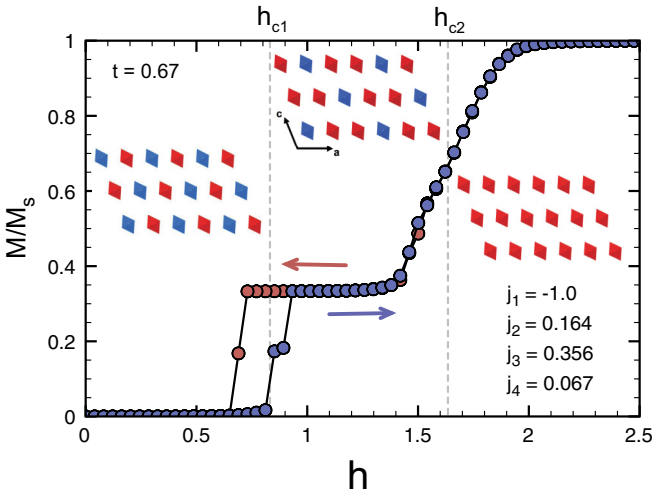

FIG. 5. (Color online) Magnetization curve obtained by Metropolis Monte Carlo calculations. The schematic structures corresponding to antiferromagnetic ($M/M_s = 0$ for $h < h_{c1}$), intermediate ($M/M_s = 1/3$ for $h_{c1} < h < h_{c2}$), and ferromagnetic ($M/M_s = 1$ for $h > h_{c2}$) orders are shown in the insets. The crystal is observed along the chain direction and red (blue) octahedra represent spin-up (spin-down) magnetic moments.

with the Hamiltonian

$$\hat{H} = \sum_{i>j} j_{ij}\sigma_i\sigma_j - h\sum_i \sigma_i, \tag{8}$$

where we have chosen $|J_1^{\parallel}|$ as the energy unit, $\sigma_i = \pm 1$ are the effective spin-1/2 variables on the Co lattice sites, j_{ij} the reduced magnetic couplings $J_i^{\parallel}/|J_1^{\parallel}|$, and $h = g\mu_B H/|J_1^{\parallel}|$ the adimensional Zeeman term representing the interaction with an external magnetic field H oriented along the easy axis.

The magnetization curve obtained from Monte Carlo simulations and the Metropolis algorithm on a system of 720 spins for a reduced temperature $t = 0.67$ is shown in Fig. 5. These results clearly show (i) the presence of the antiferromagnetic ground-state structure described above for external fields $h < h_{c1}$ and (ii) the occurrence of a phase corresponding to a 1/3 magnetization plateau between critical fields h_{c1} and h_{c2} and characterized by a $\uparrow\uparrow\downarrow$ order of the neighboring chains along a and c. These results are in agreement with the experimental magnetic structure determined very recently by Markkula and co-workers.[20]

IV. SUMMARY

In summary, our calculations show that α-CoV_2O_6 is a strongly anisotropic system favoring an orientation of the spins close to the c axis. Its magnetic interactions are those of a system of ferromagnetic Ising chains coupled on a weaker anisotropic ($J_2^{\parallel} \neq J_3^{\parallel} \neq J_4^{\parallel}$) antiferromagnetic triangular lattice leading simultaneously to the stabilization of a ground-state antiferromagnetic order and to the occurrence of an $M = 1/3$ phase under finite external fields through global spin flip of ferromagnetic chains. The antiferromagnetic ground state and our prediction for the $M = 1/3$ plateau are in agreement with the magnetic structures determined very recently by neutron diffraction experiments as reported in Refs. 17 and 20, respectively.

ACKNOWLEDGMENTS

We would like to acknowledge fruitful discussions with Vincent Robert (IPCMS, Strasbourg) and Roland Hayn (IM2NP, Marseille).

*saul@cinam.univ-mrs.fr
†Present address: IMPMC-CNRS UMR 7590, Université Pierre et Marie Curie, Campus Jussieu, 4 place Jussieu F-75252 Paris Cedex 05, France.

[1] R. Coldea *et al.*, Science **327**, 177 (2010).
[2] S. Lee *et al.*, Nat. Phys. **6**, 702 (2010).
[3] M. Belaïche *et al.*, Physica B **305**, 270 (2001).
[4] Z. He *et al.*, J. Am. Chem. Soc. **131**, 7554 (2009).
[5] M. Lenertz *et al.*, J. Phys. Chem. C **115**, 17190 (2011).
[6] S. A. J. Kimber, H. Mutka, T. Chatterji, T. Hofmann, P. F. Henry, H. N. Bordallo, D. N. Argyriou, and J. P. Attfield, Phys. Rev. B **84**, 104425 (2011).
[7] K. Singh *et al.*, J. Mater. Chem. **22**, 6436 (2012).
[8] B. Jasper-Tönnies and Hk. Müller-Bushbaum, Z. Anorg. Allg. Chem. **508**, 7 (1984).
[9] Hk. Müller-Bushbaum and M. Kobel, J. Alloys Compd. **176**, 39 (1991).
[10] A. Abragam and M. H. L. Pryce, Proc. R. Soc. London, Ser. A **206**, 173 (1951).
[11] M. E. Lines, Phys. Rev. **131**, 546 (1963).
[12] T. Oguchi, J. Phys. Soc. Jpn. **20**, 2236 (1965).
[13] P. Blaha, K. Schwarz, G. Madsen, D. Kvaniscka, and J. Luitz, computer code WIEN2K, An Augmented Plane Wave Plus Local Orbitals Program for Calculating Crystal Properties, edited by K. Schwarz (Vienna University of Technology, Vienna, Austria, 2001).
[14] J. P. Perdew, K. Burke, and M. Ernzerhof, Phys. Rev. Lett. **77**, 3865 (1996).
[15] J. Kuneš, P. Novak, M. Divis, and P. M. Oppeneer, Phys. Rev. B **63**, 205111 (2001), and references therein.
[16] M. S. S. Brooks, Physica B **130**, 6 (1985).
[17] M. Markkula *et al.*, J. Solid State Chem. **192**, 390 (2012).
[18] A. Saúl and G. Radtke, Phys. Rev. Lett. **106**, 177203 (2011).
[19] X. Yao, J. Phys. Chem. A **116**, 2278 (2012).
[20] M. Markkula, A. M. Arévalo-López, and J. P. Attfield, Phys. Rev. B **86**, 134401 (2012).